Korea-Australia Rheology Journal, 29(3), 185-193 (August 2017) www.springer.com/13367
DOI: 10.1007/s13367-017-0019-x

# Prediction of rheology of shear thickening fluids using phenomenological and artificial neural network models

**Sanchi Arora*, Animesh Laha, Abhijit Majumdar and Bhupendra Singh Butola**
*Department of Textile Technology, Indian Institute of Technology, Delhi 110016, India*
(Received March 17, 2017; final revision received July 9, 2017; accepted July 21, 2017)

Prediction models for the viscosity curve of a shear thickening fluid (STF) over a wide range of shear rate at different temperatures were developed using phenomenological and artificial neural network (ANN) models. STF containing 65% (w/w) silica nanoparticles was prepared using polyethylene glycol (PEG) as dispersion medium, and tested for rheological behavior at different temperatures. The experimental data set was divided into training data and testing data for the model development and validation, respectively. For both the models, the viscosity of STF was estimated for all the zones with good fit between experimental and predicted viscosity, for both training and testing data sets.

***Keywords***: shear thickening fluid, rheology, prediction, modeling, artificial neural network

## 1. Introduction

Fluids can be typically categorized as Newtonian and non-Newtonian based on their relationship between shear stress and shear rate. Newtonian fluids are the ones that exhibit linear relationship between these two parameters, whereas for the non-Newtonian fluids, this relationship is non-linear (Bird *et al.*, 1960; Skelland, 1967). Amongst several kinds of non-Newtonian fluids, shear thickening fluids (STFs) have been in limelight in the last few decades because of their application in impact resistant materials (Lee *et al.*, 2003; Srivastava *et al.*, 2012; Hasanzadeh and Mottaghitalab, 2014; Galindo-Rosales *et al.*, 2015). According to the British Standard Rheological Nomenclature, shear thickening is defined as the increase in viscosity with increase in shear rate (Barnes, 1989). The physics behind this phenomenon has been explored widely with the help of modern rheo-optical devices (Brown and Jaeger, 2011), scattering techniques, Stokesian dynamic simulations, *etc*. (Bender and Wagner, 1995; Boersma *et al*., 1992; Maranzano and Wagner, 2002; Raghavan *et al*., 2000; Raghavan and Khan, 1995). At first, order-disorder transition theory was believed to be the reason behind shear thickening (Hoffman, 1998), but later, Luan *et al.* (1992) used Stokesian dynamic simulations to prove that the increase in viscosity occurs due to the formation of hydroclusters, *i.e.* jamming clusters bound together by hydrodynamic lubrication forces. There are two kinds of shear thickening behaviours: continuous shear thickening and discontinuous shear thickening (Brown and Jaeger, 2014; Galindo-Rosales, 2016). The former is observed when the volume fraction of solid is moderate (0.3-0.4). In contrast, discontinuous shear thickening, characterized by sudden jump in viscosity by orders of magnitude beyond a critical shear rate, is observed in densely packed suspensions *i.e.* volume fraction of solid $\approx 0.6$.

When an STF encounters a high speed impact situation, the apparent change in its viscosity is so drastic or discontinuous that the state of matter transforms from liquid-suspension to solid: the transition being reversible upon removal of impact (Kang *et al.*, 2010; Zhang *et al*., 2008). Owing to this property, STFs are finding applications in improving ballistic protection performance and stab resistance of soft body armor (Lee *et al*., 2002; Gurgen and Kuşhan, 2017; Srivastava *et al*., 2011; Zielinska *et al*., 2014). Since the users of these armor, *i.e.* military personnel, police, soldiers in the battlefield, security guards, *etc*. are expected to perform in any environmental condition, it is extremely necessary to investigate the rheological behavior of STF at various temperatures and shear rates. This will be helpful to predict the behaviour of STF reinforced fabric composites at different temperatures. However, development of rheological model for STF is not simple owing to a peculiar behavior exhibited by STFs across a wide range of shear rate, wherein the two rheological phenomena like shear thinning and shear thickening occur.

Many studies have been conducted to model and simulate both the phenomena of shear thinning (Al-Zahrani, 1997; Al-Zahrani and Al-Fariss, 1998; Li and Zhang, 2003) and shear thickening (Bender and Wagner, 1996; Jiang *et al*., 2003; Head *et al*., 2001), individually. In other words, all these classical models are capable of describing only a continuous course of viscosity with respect to shear rate. However, materials like STF exhibit complicated characteristics like discontinuous shear thickening. Unfortunately, there is dearth of efforts for developing analytical

*Corresponding author; E-mail: ttz148146@textile.iitd.ac.in

 

or intelligent models potent of predicting the whole viscosity curve of STFs *i.e.*, curve inclusive of shear thinning zones preceding and succeeding the discontinuous shear thickening zone (David *et al.*, 2013; Khandavalli *et al.*, 2015; Perlácová and Průša, 2015). Moreover, the relationship between viscosity and shear rate does not follow a continuous function over the entire domain of shear rate. In 2011, Galindo-Rosales *et al.* (2011a) proposed an apparent viscosity function that could provide an excellent fit to several experimental data sets. Further, Tian *et al.* (2015) extended Galindo-Rosales' study and proposed a generalized viscosity function capable of predicting the viscosity of an STF at varying temperatures and different concentrations of fumed silica. The advantage of such process models is that they extend an opportunity to generalize the experimental findings and hence help avoid conducting additional rheological experiments. However, phenomenological models involve large number of parameters and they do not explain the physics behind that relationship.

In recent years, intelligent models like artificial neural networks (ANN), fuzzy logic (FL), and genetic algorithms (GA) have been used to model and optimize highly complex and nonlinear systems. These models are proficient in mapping complex mathematical relationships between process parameters even with noisy or incomplete data (Majumdar, 2011). Interestingly, in the last two years, a lot of articles have been published reporting the prediction of viscosity and thermo-physical properties of nanofluids using ANN. Heidari *et al.* (2016) developed a feed-forward ANN model to predict nanofluid viscosity using temperature, nanoparticle size, density, volume fraction, and base fluid viscosity as input parameters. Esfe *et al.* (2015) designed an ANN that could predict thermal conductivity and dynamic viscosity of ferromagnetic nanofluids using temperature, diameter of particles, and solid volume fraction as input. A new viscosity prediction approach based on radial basis function (RBF) neural networks was proposed by Zhao *et al.* (2015), taking into account the effects of nanoparticle volume concentration, nanoparticle diameter, nanoparticle density, the viscosity of base fluid, and temperature; and was found to outperform many existing theoretical and empirical models. A comprehensive critical review of numerous theoretical, empirical, and numerical models developed for the effective viscosity of nanofluids, has been compiled by Meyer *et al.* (2016).

Though STF has received considerable attention from the researchers for developing impact resistant materials, there has been no published research that explores the rheological modeling of STF using ANN. An attempt has been made in this research to develop predictive models for discontinuous shear viscosity of STF at various shear rates and temperatures using phenomenological and ANN models and compare their prediction accuracy.

## 2. Experimental

### 2.1. Synthesis of STF

Colloidal silica nano-particles MP1040 of size 100 nm were obtained in water-suspension (40% w/w) form, from Nissan Chemicals, Japan. Polyethylene glycol or PEG (200 $M_w$) was added to silica-water suspension in requisite quantity so that 65% w/w STF is obtained after the evaporation of water. The water content from the mixture of Si-water suspension and PEG was evaporated by ultrasonicating it at 650 W in Elmasonic S 60 H Ultrasonicator at 60°C for about 8 h. Silica concentration exceeding 65% w/w was not used for STF preparation as the fluid became very viscous while water evaporation.

### 2.2. Rheological analysis of STF

Stress controlled rheometer (Anton Paar Physica MCR 51) was used for the rheological characterization of the prepared STF. Parallel plate geometry was used and a gap of 0.5 mm was maintained between two parallel plates. Diameter of the upper plate was 25 mm. STF was placed between the two parallel plates and shear rate was varied from 0 to 700 $s^{-1}$. The viscosity vs. shear rate behavior of STF was recorded at six different temperatures *i.e.* 5°C, 10°C, 15°C, 20°C, 25°C, and 30°C. Temperature was maintained at desired level by Peltier temperature control system of rheometer.

### 2.3. Methodology for phenomenological model development

#### 2.3.1. Galindo-Rosales' model

The typical rheological behavior of STF is shown in Fig. 1. At low shear rates, the viscosity is seen to follow a decreasing trend with the increase in shear rate, also known as shear thinning (Zone I). This continues until the shear rate reaches a critical value $\dot{\gamma}_c$, where the viscosity is seen to attain its lowest value $\eta_c$. Thereafter, the viscosity starts to shoot up dramatically at higher shear rates (shear thickening), until it reaches its peak value $\eta_{max}$ at shear rate $\dot{\gamma}_{max}$ (Zone II). At even higher shear rates, the material begins to exhibit shear thinning behavior again (Zone III).

In general, power-law model (Eq. (1)) is used for the determination of rheological behavior of an STF.

$$\eta(\dot{\gamma}) = m\dot{\gamma}^{n-1}. \quad (1)$$

Although, this model fits well for the interval of shear rate where viscosity increases with respect to increase in shear rate, *i.e.* $n > 1$, it is not suitable to be used for the low and high shear rate regions where shear thinning occurs (Macosko, 1994). To address this problem, Galindo-

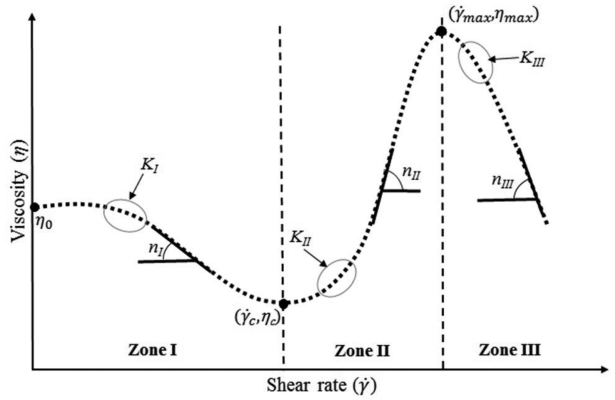


**Fig. 1.** Typical rheological behavior of an STF.

Rosales *et al.* (2011b) proposed to build an apparent viscosity prediction function for the complete viscosity curve of an STF using piecewise definitions for the three different regions of shear rate as shown in Eq. (2).

$$\eta(\dot{\gamma}) = \begin{cases} \eta_I(\dot{\gamma}) & \text{for} \quad \dot{\gamma} \le \dot{\gamma}_c \\ \eta_{II}(\dot{\gamma}) & \text{for} \quad \dot{\gamma}_c < \dot{\gamma} \le \dot{\gamma}_{\max} \\ \eta_{III}(\dot{\gamma}) & \text{for} \quad \dot{\gamma}_{\max} < \dot{\gamma} \end{cases} \tag{2}$$

where, $\dot{\gamma}$ is the viscosity function that fits the zone $i$ ($i = I$, $II$, $III$) of the general viscosity curve as represented in Fig. 1. It was considered that a function with shape similar to the Cross' model (Eq. (3)) be developed to depict the three zones.

$$\eta(\dot{\gamma}) = \eta_\infty + \frac{\eta_0 - \eta_\infty}{1 + (K\dot{\gamma})^n}. \tag{3}$$

Here, $\eta_0$ and $\eta_\infty$ are representative of the asymptotic values of viscosity at very low and very high shear rates, respectively; $K$ is a constant with dimension of time and corresponds to the shape of the curve in the transition from the plateau $\eta_\infty$ to power-law, and further from power-law to plateau $\eta_0$; and $n$ is a dimensionless constant corresponding to the slope of the power-law region in a log-log plot. The final function developed (Eq. (4)), using Eqs. (2) and (3), comprised of the eleven basic parameters of the viscosity curve explained as follows:

*Zone I*: Shear thinning zone, where $\eta_0$ is the asymptotic viscosity value at very low shear rates; $n_I$ depicts the slope of the curve in log-log plot; $K_I$ determines the transition between the plateau and the power-law; and $\eta_c$ refers to the plateau at which Zone *I* terminates.

*Zone II*: Shear thickening zone, where $\eta_c$ shows the onset of this zone; $n_{II}$ depicts the slope of the curve in log-log plot; $K_{II}$ determines the transition between the plateau and the power-law; and $\eta_{\max}$ refers to the maximum viscosity attained at the termination of Zone *II*.

*Zone III*: Shear thinning zone, where $\eta_{\max}$ shows the onset of this zone; $n_{III}$ depicts the slope of the curve in log-log plot; $K_{III}$ determines the transition between the plateau and the power-law.

$$\eta(\dot{\gamma}) = \begin{cases} \eta_I(\dot{\gamma}) = \eta_c + \dfrac{\eta_0 - \eta_c}{1 + \left|[K_1(\dot{\gamma}^2/(\dot{\gamma} - \dot{\gamma}_c))]\right|^{n_I}} & \text{for } \dot{\gamma} \le \dot{\gamma}_c \\ \eta_{II}(\dot{\gamma}) = \eta_{\max} + \dfrac{\eta_c - \eta_{\max}}{1 + \left|[K_2((\dot{\gamma} - \dot{\gamma}_c)/(\dot{\gamma} - \dot{\gamma}_{\max}))\dot{\gamma}]\right|^{n_{II}}} & \text{for } \dot{\gamma}_c < \dot{\gamma} \le \dot{\gamma}_{\max}. \\ \eta_{III}(\dot{\gamma}) = \dfrac{\eta_{\max}}{1 + \left|[K_3(\dot{\gamma} - \dot{\gamma}_{\max})]\right|^{n_{III}}} & \text{for } \dot{\gamma}_{\max} < \dot{\gamma} \end{cases} \tag{4}$$

This proposed function (Galindo-Rosales *et al.*, 2011b) is suitable for curve fitting procedures and numerical simulations, and has been explored in this study to predict the viscosity curve of an STF with 65% solid content of silica in PEG, at various temperatures, using experimental rheological data of the same.

### 2.3.2. Data sorting and trend analysis

The entire data set, *i.e.* viscosity vs. shear rate was segregated into two categories: Training data set (10°C, 20°C, and 30°C) and testing data set (15°C and 25°C). Training data are used for estimating the model parameters whereas testing data are used for model validation. The values of viscosity at very low shear rate ($\eta_0$), critical shear rate ($\dot{\gamma}_c$), viscosity at critical shear rate ($\eta_c$), maximum viscosity ($\eta_{\max}$), and shear rate corresponding to maximum viscosity ($\dot{\gamma}_{\max}$) were noted for the training data set, as given in Table 1. It is observed that initial viscosity, critical viscosity, and maximum viscosity decrease with increase in temperature. On the other hand, critical shear rate and shear rate for attaining maximum viscosity

**Table 1.** Rheological analysis of STF for training data set.

| Temperature ($T$) [°C] | Viscosity at very low shear rate ($\eta_0$) [Pa.s] | Critical viscosity ($\eta_c$) [Pa.s] | Critical shear rate ($\dot{\gamma}_c$) [$s^{-1}$] | Maximum viscosity ($\eta_{\max}$) [Pa.s] | Shear rate at maximum viscosity ($\dot{\gamma}_{\max}$) [$s^{-1}$] |
|---|---|---|---|---|---|
| 10 | 27.10 | 8.90 | 39.50 | 194.00 | 119.00 |
| 20 | 10.57 | 6.85 | 66.70 | 149.36 | 156.00 |
| 30 | 7.31 | 3.59 | 94.80 | 112.78 | 227.00 |

increase with increase in temperature. Our observations are in agreement with the findings of Gürgen *et al.* (2016a; 2016b) who found that initial viscosity reduces and critical shear rate increases at elevated temperature as the repulsive forces between the particles increases. Therefore, higher shear rate is required for the formation of hydro-clusters. Liu *et al.* (2015) also reported that critical shear rate increases monotonically with temperature.

Using curve fitting, all these aforementioned parameters were converted to functions of temperature, represented by the following equations:

$$\dot{\gamma}_c = 2.76T + 11.833, \quad (5)$$

$$\dot{\gamma}_{\max} = 017T^2 - 1.4T + 116, \quad (6)$$

$$\eta_0 = 0.0664T^2 - 3.6435T + 56.9, \quad (7)$$

$$\eta_c = -0.0061T^2 - 0.0235T + 9.74, \quad (8)$$

$$\eta_{\max} = 0.0403T^2 - 5.673T + 246.7. \quad (9)$$

### 2.3.3. Application of Galindo Rosales' model

Six parameters of Eq. (4), *i.e.* $K_I$, $K_{II}$, $K_{III}$, $n_I$, $n_{II}$, and $n_{III}$ were determined for all training temperatures (10°C, 20°C, and 30°C), from the experimental data set, using Levenberg Marquardt Algorithm and Least Angle Regression Algorithm, by an iterative SSE (sum of squared errors) minimization technique in MATLAB® (version R2013a, MathWorks, Inc., Natick, MA, USA). Thereafter, these parameters were converted into functions of temperature (Eqs. (10) to (15)) by curve fitting using the estimated values reported in Table 2.

$$K_I = 0.0006T^2 - 0.0228T + 0.2487, \quad (10)$$

$$K_{II} = 5e^{-5}T^2 - 0.0016T + 0.0172, \quad (11)$$

$$K_{III} = 2e^{-6}T^2 - 0.0002T + 0.006, \quad (12)$$

$$n_I = 0.0094T^2 - 0.4907T + 6.9751, \quad (13)$$

$$n_{II} = 0.0031T^2 - 0.1116T + 2.819, \quad (14)$$

$$n_{III} = 0.002T^2 - 0.003T + 0.8196. \quad (15)$$

Substituting Eqs. (5) to (15) in Eq. (4), the apparent viscosity function proposed by Galindo-Rosales reduces to a function of single parameter *i.e.* temperature ($T$), as represented by Eq. (16).

$$\eta(\dot{\gamma}) = \begin{cases} \eta_I(\dot{\gamma}) & \text{for } \dot{\gamma} \le (2.76T+11.833) \\ \eta_{II}(\dot{\gamma}) & \text{for } (2.76T+11.833) < \dot{\gamma} \le (0.17T^2-1.4T+116) \\ \eta_{III}(\dot{\gamma}) & \text{for } (0.17T^2-1.4T+116) < \dot{\gamma} \end{cases} \quad (16)$$

where,

$$\eta_I = (-0.006T^2 - 0.024T + 9.74) + \frac{(0.073T^2 - 3.62T + 47.16)}{1 + \left| \frac{(0.001T^2 - 0.023T + 0.249)\dot{\gamma}^2}{(\dot{\gamma} - 2.76T - 11.833)} \right|^{(0.01T^2 - 0.491T + 6.975)}},$$

$$\eta_{II} = (0.04T^2 - 5.673T + 246.7) + \frac{(0.046T^2 + 5.65T - 236.96)}{1 + \left| \frac{(5e^{-5}T^2 - 0.002T + 0.017)\dot{\gamma}^{(0.003T^2 - 0.112T + 2.819)}}{(\dot{\gamma} - 2.76T - 11.833)} \right|^{(\dot{\gamma} - 0.17T^2 + 1.4T - 116)}},$$

$$\eta_{III} = \frac{0.04T^2 + 5.673T - 246.7}{1 + \left| \frac{(2e^{-6}T^2 - 0.0002T + 0.006)}{(\dot{\gamma} - 0.17T^2 + 1.4T - 116)} \right|^{(0.0002T^2 - 0.003T + 0.82)}}.$$

Thus, viscosity of an STF of a particular concentration can be effectively predicted for any value of shear rate at any temperature within the experimental range.

## 2.4. Methodology for artificial neural network modeling

### 2.4.1. Basics of artificial neural network (ANN)

ANN is a type of modeling technique that can mimic the behavior of human brain using simple mathematical functions. It is preferred for its adaptability due to the use of a generalization technique rather than memorization (Ramzi *et al.*, 2015). The most widely used ANN is multilayer feed forward perceptron wherein the computing elements, called neurons or nodes, are arranged into three layers: input, hidden, and output. The neurons of all these layers work in parallel path to map the mathematical relationship between input and output parameters based on experimental data sets. The number of input and output neurons corresponds to the number of input variables and the target output variables, respectively. Between these two layers, there exists at least one hidden layer that may contain any number of neurons depending upon the complexity of the function to be mapped. The determination of the optimum number of hidden layer neurons is mostly done by trial and error approach. Each neuron receives a signal from the neurons of the preceding layer, and each signal is multiplied by an interconnection weight, known

**Table 2.** Estimated values of the parameters of the viscosity function.

| Temperature [°C] | $K_I$ [s] | $K_{II}$ [s] | $K_{III}$ [s] | $n_I$ [-] | $n_{II}$ [-] | $n_{III}$ [-] |
|---|---|---|---|---|---|---|
| 10 | 0.0785 | 0.0061 | 0.0042 | 3.0070 | 2.0150 | 0.8705 |
| 20 | 0.0246 | 0.0049 | 0.0028 | 0.9166 | 1.8340 | 0.9633 |
| 30 | 0.0868 | 0.0134 | 0.0020 | 0.7039 | 2.2760 | 1.0980 |

as the synaptic weight. The weighted inputs are summed up along with a bias weight and passed through a transfer function whose output becomes the input for the neurons of the succeeding layer, until the final output is obtained by the neurons of the output layer. The prediction efficiency of an ANN depends upon the optimization of the weights *i.e.* training process for which several algorithms are available. In the present work, Levenberg Marquardt Algorithm has been used, which is based on back propagation supervised learning method wherein training occurs in two passes: forward pass and backward pass. In the forward pass, a set of experimental data is fed to the neural network and output is produced at the output nodes. Thereafter, the error vector is calculated using Eqs. (17) and (18),

$$E = \sum_{j=1}^{P} E_j , \tag{17}$$

$$E_j = 1/2 \sum_{k=1}^{S} (T_k - out_k)^2 \tag{18}$$

where, $E$ is the error vector, $P$ is the total number of training patterns, $E_j$ is the error corresponding to the $j^{th}$ pattern, and $T_k$ and $out_k$ are the target and predicted outputs, respectively, at the output neuron $k$ of total $S$ neurons in the output layer.

Further, in the backward pass, the calculated error signal $E$ is propagated backwards through the network. The synaptic weights between the output and the hidden layer are adjusted using a delta rule (Eq. (19)), such that the error signal decreases in each iteration.

$$\Delta W_{jk} = -\eta[\partial E/\partial W_{jk}] \tag{19}$$

where, $W_{jk}$ refers to the weight connecting $j^{th}$ neuron of the hidden layer and $k^{th}$ neuron of the output layer, and $\Delta W_{jk}$ is the correction applied to $W_{jk}$ at a particular iteration, $\eta$ is a constant termed as the learning rate.

#### 2.4.2. ANN parameters

In the present study, an ANN model was developed for predicting the viscosity of 65% STF by writing codes in MATLAB® (version R2013a, MathWorks, Inc., Natick, MA, USA). Experimental data were collected for shear stress vs. shear rate, for 1 $s^{-1}$ to 700 $s^{-1}$, at different temperatures. The ANN architecture has been schematically explained in Fig. 2.

Temperature and shear rate were selected as input variables, with shear stress as the target output. Considering the universal approximation theory, according to which a network with single hidden layer composed of sufficient number of neurons is potent of mapping any input to any output with reasonable degree of accuracy (Salehi and Razavi, 2012), only one hidden layer was used in this research. Tangent-sigmoid function and pure-linear transfer function were used for hidden and output layers, respectively. The training of the ANN was done for 200 iterations. Several ANN model configurations were evaluated with different number of neurons in the hidden layer so as to determine the best network architecture for the prediction of shear stress. It was found that two neurons in hidden layer led to the best prediction performance in terms of root mean squared error (Eq. (20)).

$$\text{Root mean squared error (\%)} = \frac{\sum_{i=1}^{n} (\text{Actual value}_i - \text{Predicted value}_i)^2}{n} . \tag{20}$$

The predicted value of shear stress ($\tau$) was further used to calculate viscosity ($\eta$) of the STF corresponding to a wide range of shear rate ($\dot{\gamma}$) at different temperatures as per Eq. (21).

$$\eta = \tau/\dot{\gamma} . \tag{21}$$

Finally, the prediction capability of ANN model was compared with the experimental data at 25°C (testing data set) using the experimental data of all other temperatures (training data set) for validating the efficiency of the designed network.

## 3. Results and Discussion

### 3.1. Rheological analysis

Figure 3 shows rheological plot of 65% (w/w) STF at temperatures used for creating training data set of phenomenological model, *i.e.* 10°C, 20°C, and 30°C. It can be seen that at low shear rates, the viscosity decreases with increase in shear rate, *i.e.* shear thinning is observed. However, on reaching critical shear rate, the viscosity is seen to rise sharply with increase in shear rate, confirming shear thickening behavior. Moving further, on reaching a peak level, the viscosity again starts to fall at higher values of shear rate. Therefore, it is very evident that the relationship between the viscosity and shear rate is not linear,

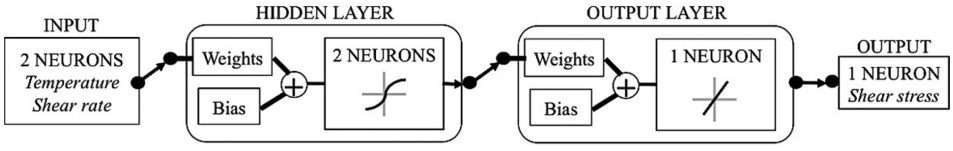


**Fig. 2.** ANN architecture designed for the prediction of shear stress of STF.

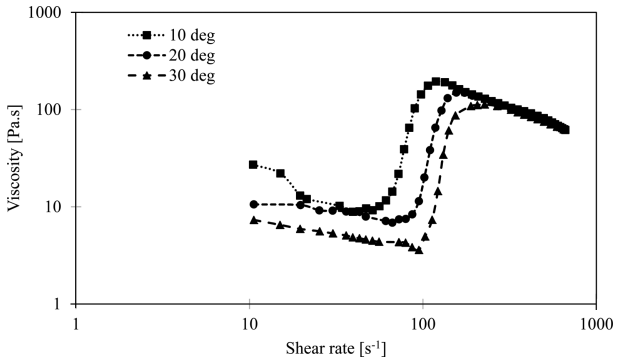


**Fig. 3.** Rheological behavior of 65% STF at different temperatures.

**Table 3.** Correlation coefficient between actual and predicted viscosities by phenomenological model.

| Data type | Temperature [°C] | Correlation coefficient |
|---|---|---|
| Training | 10 | 0.997 |
| | 20 | 0.999 |
| | 30 | 0.999 |
| Testing | 15 | 0.647 |
| | 25 | 0.969 |

and also follows the same trend at all temperatures.

### 3.2. Prediction performance of phenomenological model

The prediction accuracy of the phenomenological model is presented in Table 3. The viscosity vs. shear rate curve obtained for the complete data set using Eq. (16) has been plotted along with experimental training data, as depicted in Figs. 4a, 4b, and 4c for 10°C, 20°C, and 30°C, respectively. The critical shear rate and peak viscosity can be seen to match very well for all the three data sets. Excellent fitting between the experimental and predicted viscosity curves (correlation coefficient > 0.99), in training data sets, is expected as the experimental data were used to estimate the model parameters. However, the efficacy of the phenomenological model can be validated from its prediction performance in the testing data sets, *i.e.* 15°C and 25°C, as they were not used for model parameter estimation. The prediction performance was found to be relatively poor at 15°C as indicated by correlation coefficient of 0.647 (Fig. 5a and Table 3). Nevertheless, the predicted viscosity curve shows good association with the experimental one at 25°C (Fig. 5b) with a high correlation coefficient of 0.969.

### 3.3. Prediction performance of ANN model

The viscosity vs. shear rate curves for all temperatures from the training data set, and for test temperature 25°C, obtained by using ANN model have been plotted along

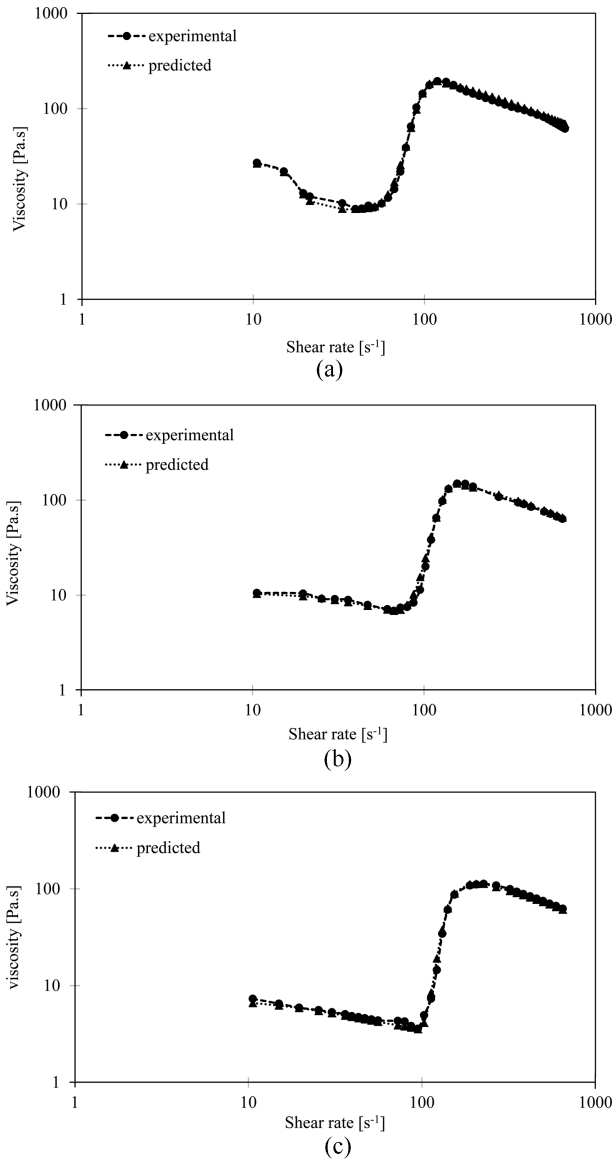


**Fig. 4.** Experimental and predicted viscosity by phenomenological model for training data sets corresponding to (a) 10°C, (b) 20°C, and (c) 30°C.

with experimental data in Fig. 6. It can be seen that the ANN model has been able to grasp the nature of the viscosity curve with the help of training data set. All the predicted viscosity graphs show a shear thinning region followed by a discontinuous shear thickening and finally a shear thinning. The correlation coefficients between experimental and predicted viscosities for training data sets as well as testing data set have been presented in Table 4. The correlation coefficients are found to be good except in case of training data corresponding to 10°C. At low temperature, shear thickening is more discontinuous which may be one of the reasons for mismatch between experimental and predicted viscosity curves.

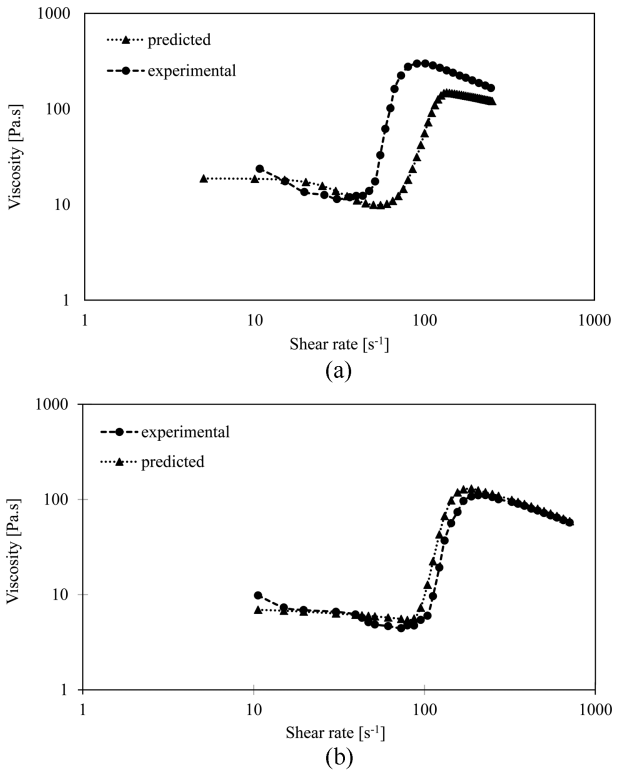


**Fig. 5.** Experimental and predicted viscosity by phenomenological model for testing data sets corresponding to (a) 15°C, and (b) 25°C.

## 4. Conclusions

The rheological behavior of STF has been predicted using phenomenological and ANN models. These models can predict the viscosity of STF at different shear rates and temperature. The apparent viscosity function of phenomenological model was based on Galindo-Rosales' approach to use piecewise functions for the prediction of viscosity in different zones of shear rate. In general, both the models were able to capture the typical nature of the viscosity-shear rate graph of STF with reasonable accuracy. Phenomenological model demonstrated excellent fit between experimental and predicted viscosity graphs (correlation coefficient > 0.99) in training data sets. Both the models showed good prediction accuracy with correlation coefficient between actual and predicted viscosity exceed-

**Table 4.** Correlation coefficient between actual and predicted viscosities by ANN model.

| Data type | Temperature [°C] | Correlation coefficient |
|---|---|---|
| Training | 10 | 0.629 |
| | 15 | 0.826 |
| | 20 | 0.976 |
| | 30 | 0.932 |
| Testing | 25 | 0.974 |

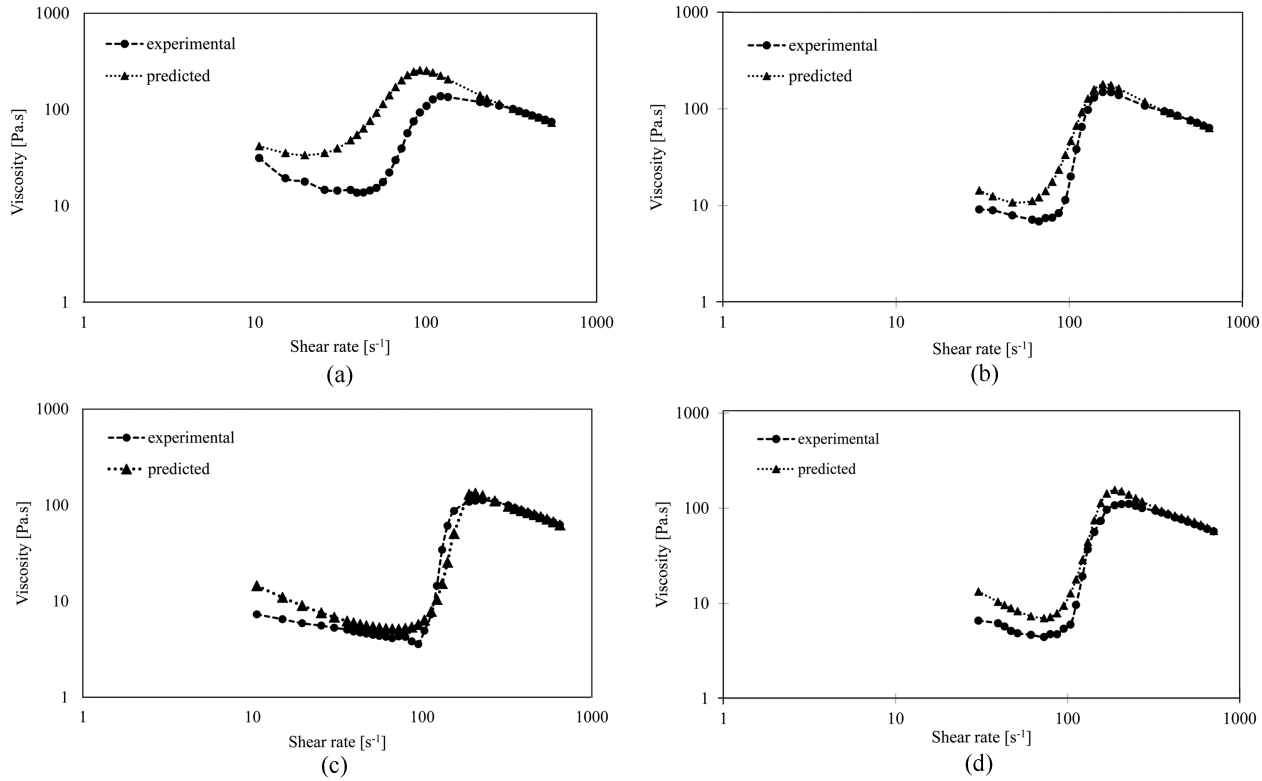


**Fig. 6.** Experimental and predicted viscosity by ANN model for training data sets (a) 10°C, (b) 20°C, (c) 30°C, and (d) testing data set 25°C.

ing 0.8, except in one temperature for each.

The phenomenological model requires eleven parameters ($\eta_0$, $\dot{\gamma}_c$, $\eta_c$, $\eta_{max}$, $\dot{\gamma}_{max}$, $K_I$, $K_{II}$, $K_{III}$, $n_I$, $n_{II}$, and $n_{III}$) as a function of temperature. Thus, it is quite intensive in terms of computation for parameter estimation. On the other hand, ANN provides a parameter free model that maps the input-output relationship based on experimental training data.

## References


Al-Zahrani, S.M., 1997, A generalized rheological model for shear thinning fluids, *J. Pet. Sci. Eng.* **17**, 211-215.

Al-Zahrani, S.M. and T.F. Al-Fariss, 1998, A general model for the viscosity of waxy oils, *Chem. Eng. Process.* **37**, 433-437.

Barnes, H.A., 1989, Shear-thickening ("Dilatancy") in suspensions of nonaggregating solid particles dispersed in Newtonian liquids, *J. Rheol.* **33**, 329-366.

Bender, J. and N.J. Wagner, 1996, Reversible shear thickening in monodisperse and bidisperse colloidal dispersions, *J. Rheol.* **40**, 899-916.

Bender, J.W. and N.J. Wagner, 1995, Optical measurement of the contributions of colloidal forces to the rheology of concentrated suspensions, *J. Colloid Interface Sci.* **172**, 171-184.

Bird, R.B., W.E. Steward, and E.W. Lightfoot, 1960, *Transport Phenomena*, 1st ed., Wiley, New York.

Boersma, W.H., J. Laven, and H.N. Stein, 1992, Viscoelastic properties of concentrated shear-thickening dispersions, *J. Colloid Interface Sci.* **149**, 10-22.

Brown, E. and H.M. Jaeger, 2011, Through thick and thin, *Science* **333**, 1230-1231.

Brown, E. and H.M. Jaeger, 2014, Shear thickening in concentrated suspensions: Phenomenology, mechanisms and relations to jamming, *Rep. Prog. Phys.* **77**, 046602.

David, J., P. Filip, and A.A. Kharlamov, 2013, Empirical modelling of nonmonotonous behaviour of shear viscosity, *Adv. Mater. Sci. Eng.* **2013**, 658187.

Esfe, M.H., S. Saedodin, N. Sina, M. Afrand, and S. Rostami, 2015, Designing an artificial neural network to predict thermal conductivity and dynamic viscosity of ferromagnetic nanofluid, *Int. Commun. Heat Mass Transf.* **68**, 50-57.

Galindo-Rosales, F.J., 2016, Complex fluids in energy dissipating systems, *Appl. Sci.-Basel* **6**, 206.

Galindo-Rosales, F.J., F.J. Rubio-Hernández, and A. Sevilla, 2011a, An apparent viscosity function for shear thickening fluids, *J. Non-Newton. Fluid Mech.* **166**, 321-325.

Galindo-Rosales, F.J., F.J. Rubio-Hernández, A. Sevilla, and R.H. Ewoldt, 2011b, How Dr. Malcom M. Cross may have tackled the development of "An apparent viscosity function for shear thickening fluids", *J. Non-Newton. Fluid Mech.* **166**, 1421-1424.

Galindo-Rosales, F.J., S. Martínez-Aranda, and L. Campo-Deaño, 2015, CorkSTFμfluidics - A novel concept for the development of eco-friendly light-weight energy absorbing composites, *Mater. Des.* **82**, 326-334.

Gürgen, S. and M.C. Kuşhan, 2017, The stab resistance of fabrics impregnated with shear thickening fluids including various particle size of additives, *Compos. Pt. A-Appl. Sci. Manuf.* **94**, 50-60.

Gürgen, S., M.C. Kuşhan, and W. Li, 2016a, The effect of carbide particle additives on rheology of shear thickening fluids, *Korea-Aust. Rheol. J.* **28**, 121-128.

Gürgen, S., W. Li, and M.C. Kuşhan, 2016b, The rheology of shear thickening fluids with various ceramic particle additives, *Mater. Des.* **104**, 312-319.

Hasanzadeh, M. and V. Mottaghitalab, 2014, The role of shear-thickening fluids (STFs) in ballistic and stab-resistance improvement of flexible armor, *J. Mater. Eng. Perform.* **23**, 1182-1196.

Head, D.A., A. Ajdari, and M.E. Cates, 2001, Jamming, hysteresis, and oscillation in scalar models for shear thickening, *Phys. Rev. E* **64**, 061509.

Heidari, E., M.A. Sobati, and S. Movahedirad, 2016, Accurate prediction of nanofluid viscosity using a multilayer perceptron artificial neural network (MLP-ANN), *Chemometrics Intell. Lab. Syst.* **155**, 73-85.

Hoffman, R.L., 1998, Explanations for the cause of shear thickening in concentrated colloidal suspensions, *J. Rheol.* **42**, 111-123.

Jiang, B., D.J. Keffer, B.J. Edwards, and J.N. Allred, 2003, Modeling shear thickening in dilute polymer solutions: Temperature, concentration, and molecular weight dependencies, *J. Appl. Polym. Sci.* **90**, 2997-3011.

Kang, T.J., K.H. Hong, and M.R. Yoo, 2010, Preparation and properties of fumed silica/kevlar composite fabrics for application of stab resistant material, *Fiber. Polym.* **11**, 719-724.

Khandavalli, S., J.A. Lee, M. Pasquali, and J.P. Rothstein, 2015, The effect of shear-thickening on liquid transfer from an idealized gravure cell, *J. Non-Newton. Fluid Mech.* **221**, 55-65.

Laun, H.M., R. Bung, S. Hess, W. Loose, O. Hess, K. Hahn, E. Hädicke, R. Hingmann, F. Schmidt, and P. Lindner, 1992, Rheological and small angle neutron scattering investigation of shear-induced particle structures of concentrated polymer dispersions submitted to plane Poiseuille and Couette flow, *J. Rheol.* **36**, 743-787.

Lee, Y.S., E.D. Wetzel, and N.J. Wagner, 2003, The ballistic impact characteristics of Kevlar® woven fabrics impregnated with a colloidal shear thickening fluid, *J. Mater. Sci.* **38**, 2825-2833.

Lee, Y.S., E.D. Wetzel, R.G. Egres, and N.J. Wagner, 2002, Advanced body armor utilizing shear thickening fluids, *23rd Army Science Conference*, Orlando, Florida.

Li, H. and J. Zhang, 2003, A generalized model for predicting non-Newtonian viscosity of waxy crudes as a function of temperature and precipitated wax, *Fuel* **82**, 1387-1397.

Liu, X.Q., R.Y. Bao, X.J. Wu, W. Yang, B.H. Xie, and M.B. Yang, 2015, Temperature induced gelation transition of a fumed silica/PEG shear thickening fluid, *RSC Adv.* **5**, 18367-18374.

Macosko, C.W., 1994, *Rheology: Principles, Measurements, and Applications*, Wiley-VCH, New York.

Majumdar, A., 2011, Soft computing in fibrous materials engineering, *Text. Prog.* **43**, 1-95.

Maranzano, B.J. and N.J. Wagner, 2002, Flow-small angle neu-

tron scattering measurements of colloidal dispersion microstructure evolution through the shear thickening transition, *J. Chem. Phys.* **117**, 10291-10302.

Meyer, J.P., S.A. Adio, M. Sharifpur, and P.N. Nwosu, 2016, The viscosity of nanofluids: A Review of the theoretical, empirical, and numerical models, *Heat Transf. Eng.* **37**, 387-421.

Perlácová, T. and V. Průša, 2015, Tensorial implicit constitutive relations in mechanics of incompressible non-Newtonian fluids, *J. Non-Newton. Fluid Mech.* **216**, 13-21.

Raghavan, S.R., J. Hou, G.L. Baker, and S.A. Khan, 2000, Colloidal interactions between particles with tethered nonpolar chains dispersed in polar media: Direct correlation between dynamic rheology and interaction parameters, *Langmuir* **16**, 1066-1077.

Raghavan, S.R. and S.A. Khan, 1995, Shear-induced microstructural changes in flocculated suspensions of fumed silica, *J. Rheol.* **39**, 1311-1325.

Ramzi, M., M. Kashaninejad, F. Salehi, A.R.S. Mahoonak, and S.M.A. Razavi, 2015, Modeling of rheological behavior of honey using genetic algorithm-artificial neural network and adaptive neuro-fuzzy inference system, *Food Biosci.* **9**, 60-67.

Salehi, F. and S.M.A. Razavi, 2012, Dynamic modeling of flux and total hydraulic resistance in nanofiltration treatment of regeneration waste brine using artificial neural networks, *Desalin. Water Treat.* **41**, 95-104.

Skelland, A.H.P., 1967, *Non-Newtonian Flow and Heat Transfer*, Wiley, New York.

Srivastava, A., A. Majumdar, and B.S. Butola, 2011, Improving the impact resistance performance of Kevlar fabrics using silica based shear thickening fluid, *Mater. Sci. Eng. A-Struct. Mater. Prop. Microstruct. Process.* **529**, 224-229.

Srivastava, A., A. Majumdar, and B.S. Butola, 2012, Improving the impact resistance of textile structures by using shear thickening fluids: A review, *Crit. Rev. Solid State Mat. Sci.* **37**, 115-129.

Tian, T., G. Peng, W. Li, J. Ding, and M. Nakano, 2015, Experimental and modelling study of the effect of temperature on shear thickening fluids, *Korea-Aust. Rheol. J.* **27**, 17-24.

Zhang, X.Z., W.H. Li, and X.L. Gong, 2008, The rheology of shear thickening fluid (STF) and the dynamic performance of an STF-filled damper, *Smart Mater. Struct.* **17**, 035027.

Zhao, N., X. Wen, J. Yang, S. Li, and Z. Wang, 2015, Modeling and prediction of viscosity of water-based nanofluids by radial basis function neural networks, *Powder Technol.* **281**, 173-183.

Zielinska, D., B. Delczyk-Olejniczak, L. Wierzbicki, B. Wilbik-Hałgas, M.H. Struszczyk, and M. Leonowicz, 2014, Investigation of the effect of para-aramid fabric impregnation with shear thickening fluid on quasi-static stab resistance, *Text. Res. J.* **84**, 1569-1577.